





Effect of carrier localization on anomalous Hall effect in the structurally chiral β -Mn type $\text{Co}_7\text{Zn}_7\text{Mn}_6$ alloy

Prasanta Chowdhury ¹, Mohamad Numan ¹, Shuvankar Gupta ², Souvik Chatterjee,³
Saurav Giri,¹ and Subham Majumdar ^{1,*}

¹*School of Physical Sciences, Indian Association for the Cultivation of Science, 2A and B Raja S. C. Mullick Road, Jadavpur, Kolkata 700 032, India*

²*Condensed Matter Physics Division, Saha Institute of Nuclear Physics, 1/AF, Bidhannagar, Kolkata 700 064, India*

³*UGC-DAE Consortium for Scientific Research, Kolkata Centre, Sector III, LB-8, Salt Lake, Kolkata 700106, India*



(Received 13 September 2023; revised 27 February 2024; accepted 2 April 2024; published 18 April 2024)

The effect of carrier localization due to electron-electron interaction in the anomalous Hall effect is elusive and there are contradictory results in the literature. To address the issue, we report here the detailed transport study including the Hall measurements on β -Mn type cubic compound $\text{Co}_7\text{Zn}_7\text{Mn}_6$ with a chiral crystal structure, which lacks global mirror symmetry. The alloy orders magnetically below $T_c = 204$ K, and is reported to show spin glass state at low temperature. The longitudinal resistivity (ρ_{xx}) shows a pronounced upturn below $T_{\min} = 75$ K, which is found to be associated with carrier localization due to quantum interference effect. The upturn in ρ_{xx} shows a $T^{1/2}$ dependence and it is practically insensitive to the externally applied magnetic field, which indicates that electron-electron interaction is primarily responsible for the low- T upturn. The studied sample shows a considerable value of the anomalous Hall effect below T_c . We found that the localization effect is present in the ordinary Hall coefficient (R_0), but we failed to observe any signature of localization in the anomalous Hall resistivity or conductivity. The absence of localization effect in the anomalous Hall effect in $\text{Co}_7\text{Zn}_7\text{Mn}_6$ may be due to large carrier density, and it warrants further theoretical investigations, particularly with systems having broken mirror symmetry.

DOI: [10.1103/PhysRevB.109.134428](https://doi.org/10.1103/PhysRevB.109.134428)

I. INTRODUCTION

The ordinary Hall (OH) effect, which arises from the deflection of the moving charge carriers due to Lorentz force, was discovered in 1879 [1], and its underlying mechanism is, in general, considered to be well comprehended. In contrast, the anomalous Hall effect (AHE) [2,3] observed in magnetic materials has remained relatively subtle. The phenomenon is intriguing both from a fundamental point of view as well as for its potential applications in sensors, memories, and logics [4,5]. It is now well recognized that there are mainly three mechanisms responsible for AHE, namely, intrinsic mechanism, skew scattering, and side jump [5]. Karplus and Luttinger suggested that an intrinsic mechanism arises from transverse velocity of the Bloch electrons induced by spin-orbit interaction (SOI) and interband mixing [6] and, recently, Xiao *et al.* reinterpreted it in terms of Berry curvature of the occupied Bloch states [7]. The other two mechanisms (skew scattering and side jump) are extrinsic in nature and they arise from the asymmetric scattering of the conduction electrons by the impurities in presence of SOI as proposed by Smit [8,9] and Berger [10]. Depending upon its origin, the anomalous Hall resistivity (ρ_{xy}^{AHE}) scales differently with longitudinal resistivity (ρ_{xx}). The skew scattering is generally observed in highly conducting metals ($\rho_{xx} \lesssim 10^{-6} \Omega \text{ cm}$) with a low amount of impurities [5] and it varies as $\rho_{xy}^{\text{AHE}} \propto \rho_{xx}$. On the

other hand, both intrinsic and side-jump mechanisms follow $\rho_{xy}^{\text{AHE}} \propto \rho_{xx}^2$.

However, the situation is far more complex if a comparatively higher degree of disorder is present in the magnetic metal ($\rho_{xx} \gtrsim 10^{-3} \Omega \text{ cm}$). In the presence of disorder, the quantum effects become more prominent, and the system can show localization of charge carriers due to electron-electron coulomb interaction (EEI), disordered induced weak localization (WL), or Kondo effect [5,11,12]. As a result, metallic $\rho_{xx}(T)$ exhibits an upturn [$d\rho_{xx}(T)/dT < 0$] at low temperature (T), and a resistivity minimum (at T_{\min}) is observed [12–16]. The effect of quantum corrections has been extensively studied for longitudinal conductivity and conventional Hall effect [11,12,17], but it is still poorly understood in case of AHE.

There are few recent theoretical and experimental works addressing the effect of localization on AHE [14,16,18–27]. It is shown theoretically that WL does not contribute towards side-jump mechanism, but it can have nonzero contribution in skew scattering [18,19]. On the other hand, EEI correction to AHE identically vanishes for both skew scattering and side jump due to general symmetry reasons [19,20]. The above theoretical prediction of the absence of EEI correction towards AHE was experimentally verified in Co_2FeSi Heusler alloy thin film [13] and $\text{Zr}_{1-x}\text{V}_x\text{Co}_{1.6}\text{Sn}$ semimetal [27]. On the other hand, WL correction was experimentally observed in polycrystalline Fe, Ni, FePt, and amorphous CoFeB films [14,21–24]. However, there are some disordered systems which do not follow the above rules. For example, WL effect

*sspsm2@iacs.res.in

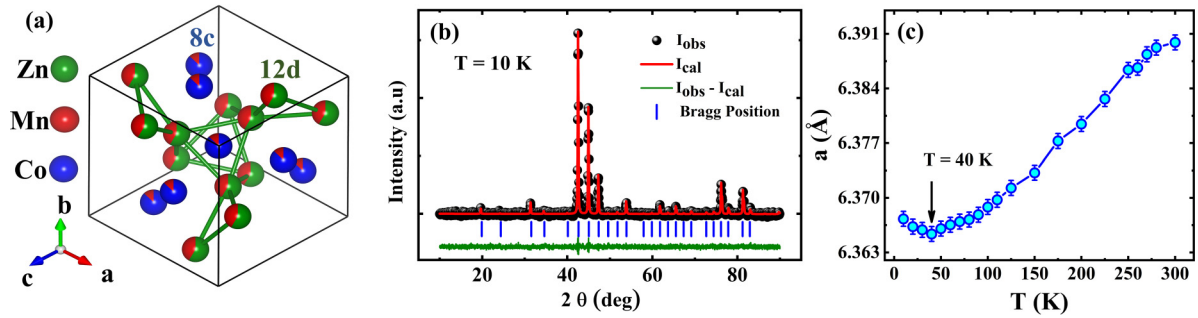


FIG. 1. (a) Crystal structure of $\text{Co}_7\text{Zn}_7\text{Mn}_6$ ($P4_132$ -right-handed structure) as viewed along the [111] direction. (b) Powder x-ray diffraction pattern of $\text{Co}_7\text{Zn}_7\text{Mn}_6$ (data points) and Rietveld refinement curves (solid line) at 10 K. (c) Thermal variation of lattice parameter (a).

in AHE is found to be absent in the disordered ferromagnets $\text{Ga}_{1-x}\text{Mn}_x\text{As}$ [16]. Similarly, a pronounced low- T EEI correction to AHE was observed in the magnetic semiconductor HgCr_2Se_4 [25]. A recent theoretical work proposed that the low- T EEI correction could exist and anomalous Hall conductivity should follow as $T^{1/2}/\ln(T_0/T)$ in three-dimensional (3D) [26] material. Therefore, the effect of disorder on AHE remains inconclusive both theoretically and experimentally.

In previous experimental works addressing the localization effect on AHE, the majority of the works have been on systems having WL. There are only a few experimental reports where EEI is the primary cause of the localization [13,25,27]. However, those few systems where EEI is prevalent, the temperature window where the upturn in $\rho_{xx}(T)$ is observed (i.e., the region where EEI mediated localization dominates) is narrow (T_{\min} is 30 K or less), and the upturn is rather weak. To examine the role of EEI in AHE, it is important to search for a system showing significant upturn in $\rho_{xx}(T)$ over a large T range. For the present paper, we chose β -Mn-type $\text{Co}_7\text{Zn}_7\text{Mn}_6$ alloy, which can be thought of being derived from $\text{Co}_{10}\text{Zn}_{10}$ by the substitution of Co and Zn by Mn. Below a critical temperature $T_c \sim 480$ K, $\text{Co}_{10}\text{Zn}_{10}$ undergoes a transition from paramagnetic state to helimagnetic state [28,29] and T_c decreases with the partial substitution of Mn. Just below T_c , it exhibits a skyrmionic state in a small T and field (H) (100 Oe $\lesssim H \lesssim 400$ Oe) windows. At higher H ($H > 1$ kOe), the sample attains a completely ferromagnetic (FM) state. This alloy has a chiral cubic crystal structure (enantiomeric space group $P4_132$ or $P4_332$, depending on its handedness) and the unit cell contain 20 atoms which are distributed over two Wyckoff sites [8c and 12d, see Fig. 1(a)] [29,30]. Previous studies revealed that 8c sites are mainly occupied by Co atoms while Zn and Mn atoms prefer the hyper kagomé network of 12d sites [31–33]. Due to multiple crystallographic sites and similar radii of Mn, Co, and Zn atoms, antisite disorder is very likely to occur in these β -Mn-type alloys [32,33]. These materials are ideal test beds for studying the disorder effect in AHE, because they show (i) long-range magnetic ordering with spontaneous magnetization and have (ii) chiral structure lacking both inversion and mirror symmetry, which can lead to intrinsic Berry phase induced Hall effect.

Until now, Co-Zn-Mn alloys were mostly studied to explore the skyrmionic state [29,34,35] via magnetization, ac susceptibility, small angle neutron scattering, and transmission electron microscopy. However, little attention has been

given to their electronic transport properties, unlike the other related skyrmionic materials, such as MnSi, where Hall conductivity is extensively studied [36–38]. In fact, previous Hall studies on Co-Zn-Mn gave some contradictory results. Zeng *et al.* reported the main mechanism behind the AHE to be skew scattering [39], while Qi *et al.* found the dominance of intrinsic mechanism [40]. In the present paper, we have carefully investigated the AHE in the alloy $\text{Co}_7\text{Zn}_7\text{Mn}_6$ with the intention to see whether the effect of carrier localization is affecting it. Our work indicates that the sample shows upturn in ρ_{xx} due to EEI, while AHE remains unaffected, which substantiates the theory proposed by Muttalib and Wölfle, and Langenfeld and Wölfle [19,20].

II. EXPERIMENTAL DETAILS

A polycrystalline sample of $\text{Co}_7\text{Zn}_7\text{Mn}_6$ was synthesized by the method as described in previous report by Karube *et al.* [34]. The structural investigation of the sample was performed by powder x-ray diffraction (PXRD) in the T range 10–300 K, using RIGAKU Smartlab (9KW) XG diffractometer fitted with a helium closed cycle refrigerator, using $\text{Cu K}\alpha$ radiation. The Rietveld refinement of the XRD data was performed using the MAUD software package [41]. Magnetic measurements were carried out using the vibrating sample magnetometer module of a commercial physical properties measurement system (PPMS, Quantum Design) as well as on a SQUID-VSM (MPMS3) of Quantum Design. The standard four-probe technique was used to measure ρ_{xx} on a cryogenic high magnetic field system (Cryogenic Ltd. UK) between 5 and 300 K. Hall measurements were performed using Physical Properties Measurement System (Quantum design Inc., USA) using four probe technique.

III. RESULTS

A. Powder x-ray diffraction

The Rietveld refinement of the temperature-dependent PXRD data indicate that the sample retains its cubic structure with space group $P4_132$, down to the lowest measured temperature of 10 K [Fig. 1(b)]. Figure 1(c) shows the thermal variation of lattice parameter a (in Å). The cubic lattice parameter a decreases monotonically down to 40 K with lowering of T . Interestingly, below 40 K, we notice a clear anomaly as a increases with decreasing T . As a result, we find

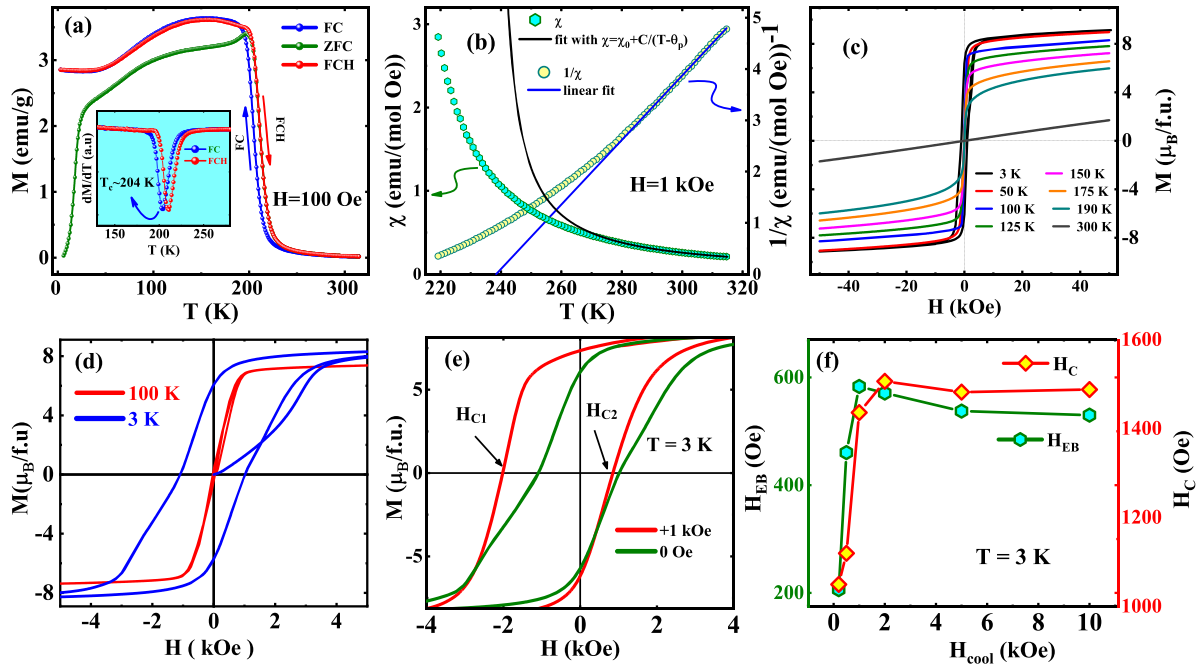


FIG. 2. (a) The magnetization (M) as a function of the temperature (T) measured in zero field-cooled-heating (ZFCH), field-cooled (FC), and field-cooled-heating (FCH) protocols under $H = 100$ Oe. The inset shows the temperature derivative of $M(T)$. (b) Susceptibility (χ) versus temperature (T) fitted with modified Curie-Weiss law (left axis) and inverse susceptibility (χ^{-1}) versus temperature (T) data with linear fitting (right axis), measured at $H = 1$ kOe. (c) Isothermal magnetization at different temperatures measured between ± 50 kOe. (d) Enlarged view of the M vs H curve at 3 K and 100 K plotted between ± 5 kOe. (e) Shows isothermal magnetization data measured at 3 K after being cooled at zero and +1 k Oe. (f) Shows the variation of exchange bias field (H_{EB}) on left axis and coercive field (H_C) on right axis as a function of cooling field (H_{cool}) at 3K.

a minimum at around 40 K in the a versus T data, and the data below 40 K show a negative thermal expansion ($da/dT < 0$).

B. Magnetization

Figure 2(a) shows the T variation of magnetization (M) in an externally applied magnetic field of $H = 100$ Oe. The measurements were performed in zero-field-cooled-heating (ZFC), field-cooling (FC) and field-cooled-heating (FCH) protocols. The T dependence of dM/dT for FC and FCH measurements is shown in the inset of Fig. 2(a). From the minimum of the dM/dT vs T plot, the transition from paramagnetic state to a helimagnetic state [28,29,42] is found to be at $T_c \sim 204$ K. Interestingly, around T_c , there is a clear thermal hysteresis between FC and FCH data which indicates a first-order-like magnetic transition. The hysteresis is present for different temperature ramping rates (5 K and 10 K per min) and also for different magnetometers (PPMS and SQUID-VSM). However, T -dependent PXRD does not show any major anomaly in a around T_c [see Fig. 1(c)] and it rules out any structural change at T_c . A sharp drop of M below 35 K is observed in the ZFC data, which matches well with the onset of the reentrant spin-glass state reported previously based on ac susceptibility measurements [32,33]. The spin-glass transition is likely due to the geometrical frustration, which is intrinsic to the β -Mn type structure, and disorder present in the system [34]. Our T -dependent PXRD [see Fig. 1(c)] result shows an anomaly in the lattice parameter below 40 K, which is close to the spin-glass freezing temperature. This may indi-

cate a close interplay between magnetic and structural aspects in the sample.

We have examined the χ^{-1} vs T data measured at $H = 1$ kOe between 220 to 315 K, and it is shown in the right panel of Fig. 2(b). χ^{-1} is seen to deviate from linearity below 285 K and from the linear fit above 285 K, we obtain the Weiss temperature (θ_p) to be 238 K, which is quite high compared to T_c . We also tried to fit the χ vs T data with modified Curie-Weiss law: $\chi = \chi_0 + C/(T - \theta_p)$, where χ_0 is a T -independent term, C is the Curie constant, and θ_p is the Weiss temperature. As we can see from the left panel of Fig. 2(b), experimental data start to deviate from the fitting below 280 K, which indicates that the sample does not obey the Curie-Weiss law. $\text{Co}_7\text{Zn}_7\text{Mn}_6$ is an itinerant magnetic system and a deviation from the Curie-Weiss law may occur [43].

The isothermal M vs H curves recorded at different constant temperatures ($T = 3$ K, 50 K, 100 K, 125 K, 150 K, 175 K, 190 K, and 300 K), between ± 50 kOe, are plotted in Fig. 2(c). M shows fairly saturating behavior with H below T_c . The saturation magnetization (M_s) takes the maximum value $9.18 \mu_B/\text{f.u.}$ at 3 K. It is evident [see Fig. 2(c)] that the sample shows finite coercive field ($H_C \sim 1$ kOe) only at 3 K, while H_C is negligible at 100 K data. This is consistent with the previous report that the hysteresis loop is only observed below the reentrant spin glass transition temperature [32].

Interestingly, we observe a virgin loop effect [44,45] at 3 K, where the virgin line lies outside the hysteresis loop [see Fig. 2(d)]. Such a virgin loop effect often occurs due to the presence of a field-induced arrested state. The sample was

earlier found to have a spin-glass-like state at low temperature, which can be responsible for the virgin loop effect [46,47].

Several spin-glass systems were found to show the exchange bias (EB) effect [48–51], which is characterized by the horizontal shift (along the H axis) of the isothermal $M - H$ curve when cooled under a field (H_{cool}) from above the magnetic transition temperature. The values of EB and H_C can be defined as $H_{\text{EB}} = -(H_{c1} + H_{c2})/2$ and $H_C = |H_{c1} - H_{c2}|/2$, where H_{c1} and H_{c2} denote the negative and positive fields at which M turns zero, respectively [52,53]. Figure 2(e) shows the $M - H$ loops at 3 K both in the ZFC ($H_{\text{cool}} = 0$) and FC ($H_{\text{cool}} = 1$ kOe) conditions. Although we recorded the data for $H = \pm 50$ kOe, an enlarged view in the region ± 4 kOe is shown for a better clarity. Clearly, the $M - H$ loop shifts asymmetrically along the field axis in the direction opposite to H_{cool} , indicating the presence of finite EB in the system. We recorded the $M - H$ loops for different values of H_{cool} , and the variation of H_{EB} and H_C with H_{cool} is shown in Fig. 2(f). H_{EB} initially rises sharply with increasing H_{cool} up to 1 kOe followed by sluggish decrease on higher fields. The maximum value of H_{EB} is found to be 580 Oe for $H_{\text{cool}} = 1$ kOe at 3 K. The antisite disorder plays an important role towards the observed EB, because it can give rise to varied magnetic interactions depending upon the metal ion and its position in the lattice [54]. H_C follows H_{cool} variation similar to H_{EB} .

C. Electrical resistivity

We have shown the T variation of zero-field resistivity [$\rho_{xx}(T, H = 0)$] in the main panel of Fig. 3(a) for $\text{Co}_7\text{Zn}_7\text{Mn}_6$ in the range $5 \text{ K} \leq T \leq 300 \text{ K}$. ρ_{xx} vs T data show a typical metallic behavior ($\frac{d\rho_{xx}}{dT} > 0$) in the high- T region. However, below 75 K, ρ_{xx} starts to rise with decreasing T , giving rise to a resistivity minimum at $T_{\text{min}} = 75 \text{ K}$. There is a change in slope at $T_c \sim 200 \text{ K}$ [see the peak in the $d\rho_{xx}/dT$ curve in the inset (i) of Fig. 3(a)], which is close to the magnetic transition temperature ($= 204 \text{ K}$).

The low- T rise can have multiple origins, such as Kondo effect, WL, or EEI [12]. Kondo effect involves $\log_{10}(T)$ upturn of $\rho_{xx}(T)$ at low temperature [55–57], which is absent in our data, and it rules out the Kondo-type localization of charge carriers. The contribution from WL to ρ_{xx} varies as $T^{p/2}$ ($p = 3/2, 2$ or 3) in 3D disordered systems [12], and it is very sensitive to H . In case of $\text{La}_{1-x}\text{A}_x\text{MnO}_3$ ($A = \text{Ca, Sr, Ba, or Pb}$), showing resistivity upturn due to WL, the minimum in ρ_{xx} shifts to lower T on application of H and it nearly vanishes for higher applied H [58,59].

Al'tshuler and Aronov have shown that EEI gives rise to increase in ρ_{xx} with decreasing T instead of usual metallic behavior [60]. In the presence of disorder, the relative change in ρ_{xx} due to EEI is estimated to be

$$\delta\rho_{xx} = \left[\frac{\rho_0 - \rho_{xx}(T)}{\rho_0} \right] \propto \frac{\sqrt{T}\tau_e}{(P_F l_e)^2}. \quad (1)$$

Here, τ_e is the characteristic mean-free time, P_F is Fermi momentum, and l_e is the mean-free path between two successive collisions. This expression is valid for $k_B T \ll \hbar/\tau_e$, and this inequality is satisfied for $T < T_{\text{min}}$. The true cause of this upturn below T_{min} is closely associated with the quantum interference effect in the presence of disorder [60–62].

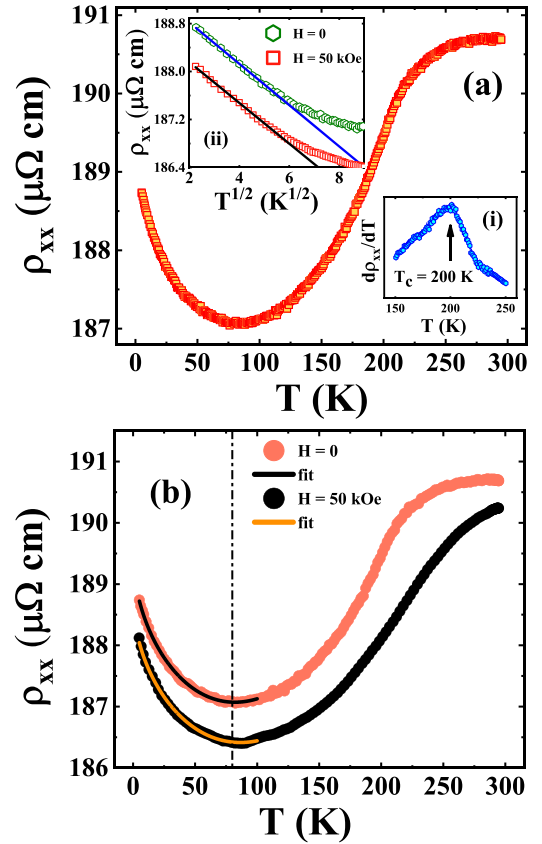


FIG. 3. (a) The T variation of resistivity (ρ_{xx}). The inset a(i) shows the $\frac{d\rho_{xx}}{dT}$ vs T curve and a(ii) shows ρ_{xx} vs $T^{1/2}$ plot below 50 K, along with a linear fit to the data. (b) ρ_{xx} vs T data at $H = 0, 50$ kOe fitted with Eq. (2).

Figure 3(b) shows the resistivity minimum of $\text{Co}_7\text{Zn}_7\text{Mn}_6$, which does not shift with H . On careful examination of the low- T part of ρ_{xx} , we find that it follows a $T^{1/2}$ dependence [see inset of Fig. 3(a)(ii)] for both $H = 0$ and 50 kOe data below about 35 K. This indicates that the EEI plays the dominant role towards the low- T upturn [62,63]. We observe that $\rho_{xx}(T, H = 50 \text{ kOe})$ lies below the zero-field counterpart due to the small but finite negative magnetoresistance (MR).

Considering all possible contributions to resistivity in our system, we model the T variation of ρ_{xx} below T_c as

$$\rho_{xx}(T, H) = \rho_{xx0} - \gamma_{\text{EEI}} T^{1/2} + \beta e^{-m} T^2 + \alpha e^{-p(T/\theta_D)^5} \int_0^{\theta_D/T} \frac{x^5 dx}{(e^x - 1)(1 - e^{-x})}. \quad (2)$$

In Eq. (2), ρ_{xx0} is a temperature independent term, while the second and the third terms, respectively, represent the electron-electron (e-e) interaction and electron-magnon (e-m) scattering contribution. The last term represents the electron-phonon (e-p) scattering contribution according to Bloch-Grüneisen model (θ_D is the Debye temperature) [64]. The continuous lines in Fig. 3(b) indicate the fitting to the data by Eq. (2) for both $H = 0$ and 50 kOe curves below 100 K. The fitting parameters are provided in Table I. We choose θ_D to be 320 K for both values of H . The coefficient

TABLE I. The fitting parameters obtained by fitting the resistivity data using Eq. (2)

H (kOe)	ρ_{xx0} ($\mu\Omega$ cm)	γEEI ($\mu\Omega$ cm $K^{-1/2}$)	β_{e-m} ($\mu\Omega$ cm K^{-2})	α_{e-p} ($\mu\Omega$ cm)
0	189.54(2)	0.36(3)	$11.7(7) \times 10^{-5}$	0.83(3)
50	188.81(3)	0.34(3)	$10.2(3) \times 10^{-5}$	0.82(8)

of electron-magnon scattering term (β_{e-m}) decreases under H , because an applied field reduces the spin-disorder scattering.

We also studied the isothermal H variation of ρ_{xx} at different T . The field variation of MR $[(\rho_{xx}(H) - \rho_{xx}(0))/\rho_{xx}(0)]$ is shown in Fig. 4(a). At 300 K, MR is found to obey an H^2 dependence [see inset of Fig. 4(b)], while MR shows a $H^{2/3}$ variation around T_c [see main panel of Fig. 4(b)]. Well below T_c (150, 120 K), a linear variation of MR with H is found [see Fig. 4(c)]. It is generally believed that for a 3d transition metal based intermetallic alloy showing FM-like order, the magnetic contribution to the resistivity arises due to the scattering of the delocalized s electrons with the partially localized 3d electrons. Under the application of H , the spin-dependent scattering diminishes, leading to negative MR.

Although the value of MR is quite small, its field variation in the different T range is quite interesting. There are several theoretical works addressing the H dependence of MR in the transition metal based itinerant magnets [65,66], and the theory predicts an $H^{2/3}$ variation around T_c [66], which is also the case for our present sample. A linear H variation

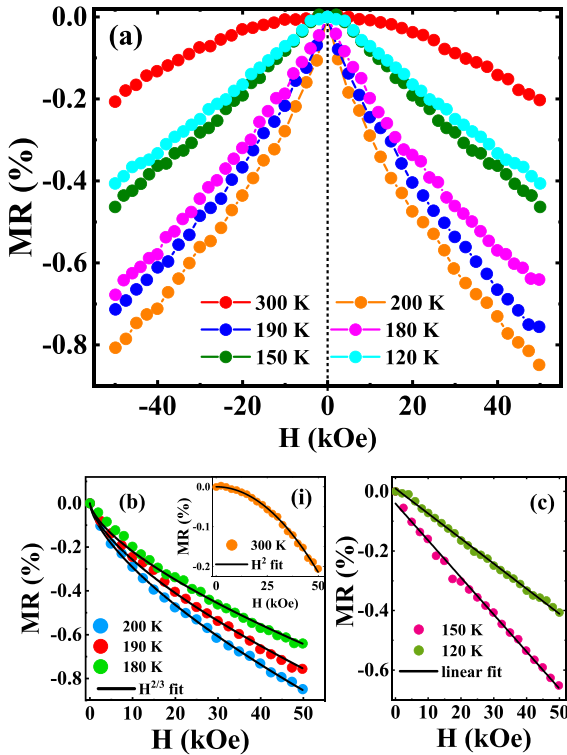


FIG. 4. (a) Isothermal field dependent MR. (b) Main panel shows $H^{2/3}$ dependence of MR vs H near the transition temperature, inset shows the H^2 dependence of MR vs H at 300 K. (c) Linear field dependence of MR well below the transition temperature.

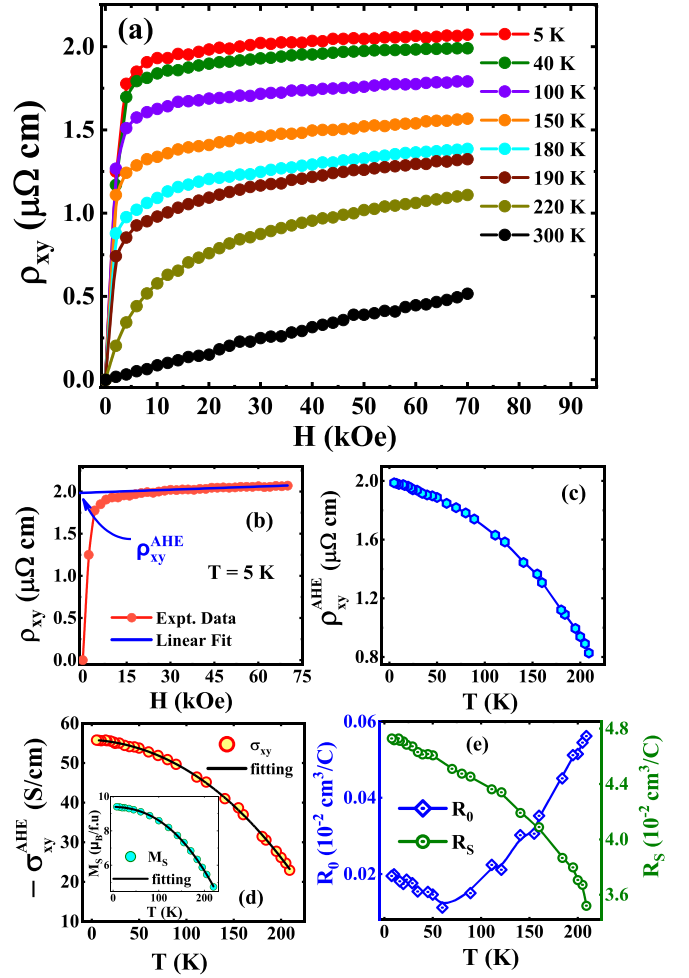


FIG. 5. (a) Hall resistivity (ρ_{xy}) vs H at different constant T . (b) ρ_{xy} vs H at $T = 5$ K with a linear fit to the high field data. (ρ_{xy}) vs H , $\rho_{xy}^{\text{AHE}}/\rho_{xx}$ vs ρ_{xx} plot with linear fit. (c) T variation of ρ_{xy}^{AHE} . (d) σ_{xy}^{AHE} vs T fitted with Eq. (4) and the inset shows the saturation magnetization (M_s) as a function of T and fitted with Eq. (4). (e) T variation of ordinary Hall coefficient (R_0) and anomalous Hall coefficient (R_s).

of MR is predicted in the $s-d$ scattering model, which is clearly observed here. The high temperature (well above T_c) H^2 variation of MR in the $s-d$ model is also evident in our 300 K data. It is clear that the observed small negative MR in the present compound arises due to the suppression of $s-d$ scattering by the applied field, and $\text{Co}_7\text{Zn}_7\text{Mn}_6$ turns out to be a classic example where the prevailing theory of MR works well at least up to 50 kOe.

D. Hall measurements

The major outcome of the present paper is based on the Hall effect study of $\text{Co}_7\text{Zn}_7\text{Mn}_6$. The Hall resistivity (ρ_{xy}) data as a function of H at various T are shown in Fig. 5(a). Here, the current is allowed to flow along the x axis, while the Hall voltage was measured along the y direction with the magnetic field along the z axis. We measured ρ_{xy} for both positive and negative values of H , and the final ρ_{xy} versus H plot was drawn using the formula $\rho_{xy}(H) =$

$\frac{1}{2}[\rho_{xy}(+H) - \rho_{xy}(-H)]$. This helps us to eliminate any MR contribution in the data. The $\rho_{xy}(H)$ is found to be highly nonlinear below about 200 K, indicating the presence of AHE. There is a sharp increase in the low field region ($H = 0 \sim 5$ kOe), and the data tend to saturate at higher fields with small positive slope. This sluggish increase in ρ_{xy} at higher H is due to the contribution from ordinary Hall effect (OHE). $\rho_{xy}(H)$ mimics the M versus H data, indicating the influence of M towards the Hall voltage. Notably, $\rho_{xy}(H)$ is linear at 300 K (well above T_c) because AHE vanishes in the paramagnetic state.

Typically, in a magnetic material with magnetization M , ρ_{xy} can be expressed as (in cgs unit)

$$\rho_{xy} = \rho_{xy}^{\text{OHE}} + \rho_{xy}^{\text{AHE}} = R_0 H + 4\pi R_S M, \quad (3)$$

where ρ_{xy}^{OHE} and ρ_{xy}^{AHE} are the ordinary and anomalous Hall resistivities with coefficients R_0 and R_S , respectively. By linear fitting the high field region ($H \geq 30$ kOe) of the ρ_{xy} vs H curve [Fig. 5(b)], we obtain ρ_{xy}^{AHE} and R_0 from the y intercept and the slope, respectively. The ρ_{xy}^{AHE} is found to decrease monotonously with increasing temperature [see Fig. 5(c)]. The anomalous Hall conductivity (σ_{xy}^{AHE}) is calculated using the formula $\sigma_{xy}^{\text{AHE}} = -\rho_{xy}^{\text{AHE}} / [(\rho_{xy}^{\text{AHE}})^2 + (\rho_{xx})^2]$ and its temperature dependence is shown in Fig. 5(d).

M_s vs T curve [see inset of Fig. 5(d)] is found to obey the well-known spin-wave (SW) equation [67,68]:

$$M_s(T) = M_s(0)(1 - AT^{3/2} - BT^{5/2}). \quad (4)$$

Here $M_s(0)$ is the value at 0 K. The fitted values of the parameters A and B are found to be $2.928 \times 10^{-5} \text{ K}^{-3/2}$ and $5.531 \times 10^{-7} \text{ K}^{-5/2}$, respectively. Interestingly, σ_{xy}^{AHE} follows a similar equation as that of Eq. (4) [i.e., $\sigma_{xy}^{\text{AHE}} \propto (1 - AT^{3/2} - BT^{5/2})$] down to 5 K without any visible anomaly below T_{min} and the corresponding fitted parameters A and B are $8.25 \times 10^{-5} \text{ K}^{-3/2}$ and $5.292 \times 10^{-7} \text{ K}^{-5/2}$, respectively. The absence of any anomaly below T_{min} indicates that both σ_{xy}^{AHE} and ρ_{xy}^{AHE} remain unaffected by the e-e localization effect present in ρ_{xx} within the accuracy of our measurements. To check the result, we measured Hall voltage using two different instruments (from Quantum Design, USA and Cryogenic Ltd, UK). However, data from both measurements are identical, providing no signature of EEI to AHE. This finding provides experimental evidence to the theoretical prediction [19,20] that the correction to σ_{xy}^{AHE} is identically zero, even though there is a finite low- T upturn in the $\rho_{xx}(T)$ data due to EEI.

Figure 5(e) shows the temperature variation of R_0 and R_S calculated using the formula $R_S = \rho_{xy}^{\text{AHE}} / (4\pi M_s)$. It is clearly seen that the localization effect is present in R_0 at low temperature but not in R_S . R_S is found to be two orders of magnitude greater than R_0 , which indicates the dominance of anomalous Hall resistivity. The coefficient R_0 is found to be positive, which indicates holes as majority charge carriers. The carrier concentration (n_h) is calculated using $n_h = 1/(R_0 e)$, and it is found to be $3.2 \times 10^{22} \text{ cm}^{-3}$ at 5 K.

IV. DISCUSSION

The most important observation from the present paper is associated with the electronic transport study of $\text{Co}_7\text{Zn}_7\text{Mn}_6$. We find a robust upturn in the longitudinal resistivity versus temperature data below about 75 K, which remains almost unaffected even under 50 kOe of field. Such low temperature upturn in otherwise metallic alloy is generally attributed to localization of charge carriers. Our careful investigation of zero field and with field $\rho_{xx}(T)$ data show that at low temperature $\rho_{xx}(T)$ follow $T^{1/2}$ dependence [see inset of Fig. 3(a)], which confirms that the electron-electron interaction is primarily responsible for this low- T upturn [12]. Evidently, this EEI mechanism is insensitive to the magnetic field (at least for $H \leq 50$ kOe).

The signature of EEI is also seen in the regular Hall coefficient, R_0 . It shows an upturn below about 70 K, which is similar to the upturn in $\rho_{xx}(T)$. A rise in R_0 also indicates a decrease in free charge carriers as $R_0 = 1/(ne)$, where n is the carrier concentration and e is the electronic charge. Interestingly, the localization effect observed in $\rho_{xx}(T)$ and R_0 at low temperature is completely absent in all components of AHE, i.e., in $\rho_{xy}^{\text{AHE}}(T)$, $R_S(T)$, and even in $\sigma_{xy}^{\text{AHE}}(T)$. As evident from Fig. 5(d), $\sigma_{xy}^{\text{AHE}}(T)$ varies monotonously and obeys the SW equation [Eq. (4)]. The fit with SW law does not show any deviation at low temperature, particularly below 75 K, where EEI localization in ρ_{xx} and R_0 is evident. This result supports the previous theoretical prediction that the EEI correction to AHE identically vanishes for both skew scattering and side-jump mechanisms [19,20]. It is to be noted that the change in the carrier concentration due to localization, as obtained from OH coefficient, is 5.57×10^{22} (at 60 K) to 3.2×10^{22} (at 5 K). Such change may not affect the electronic energy band structure required for change in anomalous Hall coefficient.

Recently, Yang *et al.* showed the presence of EEI contribution towards the AHE in the semiconducting HgCr_2Se_4 single crystal with a $T^{1/2}$ dependence of $\sigma_{xy}^{\text{AHE}}(T)$ at sub-Kelvin temperature [25]. The compound shows low- T electron localization due to EEI with $\rho_{xx}(T) \propto T^{1/2}$. The theories that rule out the contribution of EEI to AHE [19,20] assume the sample to have the mirror symmetry in its crystal structure, and consider the extrinsic mechanisms (side jump and skew scattering) only ignoring the Berry phase induced intrinsic mechanism. Yang *et al.* argued that although HgCr_2Se_4 possess overall mirror symmetry, it may be broken locally at the site of the disorder. In addition, intrinsic contribution of Hall effect may also play a role towards the observed localization effect in $\sigma_{xy}^{\text{AHE}}(T)$. The effect of EEI in $\sigma_{xy}^{\text{AHE}}(T)$ is further substantiated by a recent theoretical work [26], which proposed that $\sigma_{xy}^{\text{AHE}}(T)$ should follow $T^{1/2} / \ln(T_0/T)$ (for 3D systems) type T dependence due to the EEI effect at low- T . This theory takes into account the contribution from the Cooper channel for the purely repulsive interaction in a nonsuperconducting metal, which was overlooked in previous studies. The HgCr_2Se_4 system has relatively lower carrier density ($\sim 10^{15}$ - 10^{18} cm^{-3}) and $\rho_{xx} \sim 10^{-2} \Omega \text{ cm}$, whereas in $\text{Co}_7\text{Zn}_7\text{Mn}_6$, the carrier density is found to 10^{22} cm^{-3} and $\rho_{xx} \sim 2 \times 10^{-5} \Omega \text{ cm}$. The low carrier density in HgCr_2Se_4 may have an influence on the observed correction in $\sigma_{xy}^{\text{AHE}}(T)$.

Notably, the effect of carrier localization in AHE is also absent in Co_2FeSi thin films [13] and $\text{Zr}_{1-x}\text{V}_x\text{Co}_{1.6}\text{Sn}$ semimetal [27], which are otherwise metallic with large carrier density.

Though there is a lattice anomaly around 40 K, it is not reflected in our Hall conductivity data. The change in a is only 0.03%, which is possibly too weak to provide any detectable signature in our Hall data.

In conclusion, we fail to observe the effect of correlation-induced electron localization in the AHE in the chiral compound $\text{Co}_7\text{Zn}_7\text{Mn}_6$. Although this result is consistent with the theoretical models proposed by the group of Wölfle [19,20], it is in sharp contrast with recent experimental and theoretical works [25,26]. Most of the theories proposed so far considered the presence of mirror symmetry in the lattice and primarily concentrated on extrinsic mechanisms. Therefore, it

is important to address the issue with theoretical models where the system has broken mirror symmetry (such as the present $\text{Co}_7\text{Zn}_7\text{Mn}_6$) and with the inclusion of intrinsic contribution towards AHE.

ACKNOWLEDGMENTS

P.C. thanks the DST-INSPIRE program (Grant No. DST/INSPIRE Fellowship/2019/IF190532) for the research assistance. M.N. would like to thank CSIR, India for his research [File No. 09/080(1131)/2019-EMR-I]. The UGC DAE-CSR Kolkata center, where the low-temperature MR measurements were performed, is duly acknowledged. We thank Prof. C. Mazumdar, SINP, Kolkata for Hall measurements.

-
- [1] E. H. Hall, On a new action of the magnet on electric currents, *Am. J. Math.* **2**, 287 (1879).
- [2] E. H. Hall, On the new action of magnetism on a permanent electric current, *London, Edinburgh Dublin Philos. Mag. J. Sci.* **10**, 301 (1880).
- [3] E. H. Hall, On the rotational coefficient in nickel and cobalt, *London, Edinburgh Dublin Philos. Mag. J. Sci.* **12**, 157 (1881).
- [4] C. M. Hurd, *The Hall Effect in Metals and Alloys* (Plenum Press, New York, 1972).
- [5] N. Nagaosa, J. Sinova, S. Onoda, A. H. MacDonald, and N. P. Ong, Anomalous Hall effect, *Rev. Mod. Phys.* **82**, 1539 (2010).
- [6] R. Karplus and J. M. Luttinger, Hall effect in ferromagnetics, *Phys. Rev.* **95**, 1154 (1954).
- [7] D. Xiao, M.-C. Chang, and Q. Niu, Berry phase effects on electronic properties, *Rev. Mod. Phys.* **82**, 1959 (2010).
- [8] J. Smit, The spontaneous Hall effect in ferromagnetics I, *Physica* **21**, 877 (1955).
- [9] J. Smit, The spontaneous Hall effect in ferromagnetics II, *Physica* **24**, 39 (1958).
- [10] L. Berger, Side-jump mechanism for the Hall effect of ferromagnets, *Phys. Rev. B* **2**, 4559 (1970).
- [11] G. Bergmann, Weak localization in thin films: A time-of-flight experiment with conduction electrons, *Phys. Rep.* **107**, 1 (1984).
- [12] P. A. Lee and T. V. Ramakrishnan, Disordered electronic systems, *Rev. Mod. Phys.* **57**, 287 (1985).
- [13] B. K. Hazra, S. N. Kaul, S. Srinath, M. Manivel Raja, R. Rawat, and A. Lakhani, Evidence for the absence of electron-electron Coulomb interaction quantum correction to the anomalous Hall effect in Co_2FeSi Heusler-alloy thin films, *Phys. Rev. B* **96**, 184434 (2017).
- [14] L. Wu, K. Zhu, D. Yue, Y. Tian, and X. Jin, Anomalous Hall effect in localization regime, *Phys. Rev. B* **93**, 214418 (2016).
- [15] H. Meier, M. Yu. Kharitonov, and K. B. Efetov, Anomalous Hall effect in granular ferromagnetic metals and effects of weak localization, *Phys. Rev. B* **80**, 045122 (2009).
- [16] P. Mitra, N. Kumar, and N. Samarth, Localization and the anomalous Hall effect in a dirty metallic ferromagnet, *Phys. Rev. B* **82**, 035205 (2010).
- [17] G. Bergmann, B. L. Altshuler, and A. G. Aronov, *Electron-Electron Interactions in Disordered Systems*, edited by A. L. Efros and M. Pollak (North-Holland, Amsterdam, 1985).
- [18] V. K. Dugaev, A. Crépieux, and P. Bruno, Localization corrections to the anomalous Hall effect in a ferromagnet, *Phys. Rev. B* **64**, 104411 (2001).
- [19] K. A. Muttalib and P. Wölfle, Disorder and temperature dependence of the anomalous Hall effect in thin ferromagnetic films: Microscopic model, *Phys. Rev. B* **76**, 214415 (2007).
- [20] A. Langenfeld and P. Wölfle, Absence of quantum corrections to the anomalous Hall conductivity, *Phys. Rev. Lett.* **67**, 739 (1991).
- [21] P. Mitra, R. Mitra, A. F. Hebard, K. A. Muttalib, and P. Wölfle, Weak-localization correction to the anomalous Hall effect in polycrystalline Fe films, *Phys. Rev. Lett.* **99**, 046804 (2007).
- [22] Z. B. Guo, W. B. Mi, Q. Zhang, B. Zhang, R. O. Aboljadayel, and X. X. Zhang, Anomalous Hall effect in polycrystalline Ni films, *Solid State Commun.* **152**, 220 (2012).
- [23] Y. M. Lu, J. W. Cai, Z. Guo, and X. X. Zhang, Unconventional scaling of the anomalous Hall effect accompanying electron localization correction in the dirty regime, *Phys. Rev. B* **87**, 094405 (2013).
- [24] Y. Zhang, W. Mi, X. Wang, and Z. Guo, Scaling of anomalous Hall effect in amorphous CoFeB films with accompanying quantum correction, *Solid State Commun.* **215**, 5 (2015).
- [25] S. Yang, Z. Li, C. Lin, C. Yi, Y. Shi, D. Culcer, and Y. Li, Unconventional temperature dependence of the anomalous Hall effect in HgCr_2Se_4 , *Phys. Rev. Lett.* **123**, 096601 (2019).
- [26] S. Li and A. Levchenko, Temperature dependence of the anomalous Hall effect from electron interactions, *Phys. Rev. Lett.* **124**, 156802 (2020).
- [27] G. Wang, Z. Sun, X. Si, and S. Jia, Anomalous Hall effect in ferromagnetic Weyl semimetal candidate $\text{Zr}_{1-x}\text{V}_x\text{Co}_{1.6}\text{Sn}$, *Chin. Phys. B* **29**, 077503 (2020).
- [28] K. Karube, J. S. White, V. Ukleev, C. D. Dewhurst, R. Cubitt, A. Kikkawa, Y. Tokunaga, H. M. Rønnow, Y. Tokura, and Y. Taguchi, Metastable skyrmion lattices governed by magnetic disorder and anisotropy in β -Mn-type chiral magnets, *Phys. Rev. B* **102**, 064408 (2020).

- [29] K. Karube, J. S. White, N. Reynolds, J. L. Gavilano, H. Oike, A. Kikkawa, F. Kagawa, Y. Tokunaga, H. M. Rønnow, Y. Tokura *et al.*, Robust metastable skyrmions and their triangular-square lattice structural transition in a high-temperature chiral magnet, *Nat. Mater.* **15**, 1237 (2016).
- [30] Y. Tokunaga, X. Z. Yu, J. S. White, H. M. Rønnow, D. Morikawa, Y. Taguchi, and Y. Tokura, A new class of chiral materials hosting magnetic skyrmions beyond room temperature, *Nat. Commun.* **6**, 7638 (2015).
- [31] T. Hori, H. Shiraishi, and Y. Ishii, Magnetic properties of β -MnCoZn alloys, *J. Magn. Magn. Mater.* **310**, 1820 (2007).
- [32] J. D. Bocarsly, C. Heikes, C. M. Brown, S. D. Wilson, and R. Seshadri, Deciphering structural and magnetic disorder in the chiral skyrmion host materials $\text{Co}_x\text{Zn}_y\text{Mn}_z$ ($x + y + z = 20$), *Phys. Rev. Mater.* **3**, 014402 (2019).
- [33] T. Nakajima, K. Karube, Y. Ishikawa, M. Yonemura, N. Reynolds, J. S. White, H. M. Rønnow, A. Kikkawa, Y. Tokunaga, Y. Taguchi *et al.*, Correlation between site occupancies and spin-glass transition in skyrmion host $\text{Co}_{10-x/2}\text{Zn}_{10-x/2}\text{Mn}_x$, *Phys. Rev. B* **100**, 064407 (2019).
- [34] K. Karube, J. S. White, D. Morikawa, C. D. Dewhurst, R. Cubitt, A. Kikkawa, X. Yu, Y. Tokunaga, T.-H. Arima, H. M. Rønnow *et al.*, Disordered skyrmion phase stabilized by magnetic frustration in a chiral magnet, *Sci. Adv.* **4**, eaar7043 (2018).
- [35] D. Morikawa, X. Yu, K. Karube, Y. Tokunaga, Y. Taguchi, T.-H. Arima, and Y. Tokura, Deformation of topologically-protected supercooled skyrmions in a thin plate of chiral magnet $\text{Co}_8\text{Zn}_8\text{Mn}_4$, *Nano Lett.* **17**, 1637 (2017).
- [36] M. Lee, W. Kang, Y. Onose, Y. Tokura, and N. P. Ong, Unusual Hall effect anomaly in MnSi under pressure, *Phys. Rev. Lett.* **102**, 186601 (2009).
- [37] A. Neubauer, C. Pfleiderer, B. Binz, A. Rosch, R. Ritz, P. G. Niklowitz, and P. Boni, Topological Hall effect in the A phase of MnSi, *Phys. Rev. Lett.* **102**, 186602 (2009).
- [38] J. Zang, M. Mostovoy, J. H. Han, and N. Nagaosa, Dynamics of skyrmion crystals in metallic thin films, *Phys. Rev. Lett.* **107**, 136804 (2011).
- [39] H. Zeng, X. Zhao, G. Yua, X. Luoa, S. Maa, C. Chena, Z. Mog, Y. Zhange, Y. Chaie, J. Shen *et al.*, Magnetic and transport properties of chiral magnet $\text{Co}_7\text{Zn}_8\text{Mn}_5$, *J. Magn. Magn. Mater.* **560**, 169631 (2022).
- [40] F. Qi, Y. Huang, X. Yao, W. Lu, and G. Cao, Anomalous electrical transport and magnetic skyrmions in Mn-tuned $\text{Co}_9\text{Zn}_9\text{Mn}_2$ single crystals, *Phys. Rev. B* **107**, 115103 (2023).
- [41] L. Lutterotti, M. Bortolotti, G. Ischia, I. Lonardelli, and H.-R. Wenk, Rietveld texture analysis from diffraction images, *Z. Kristallogr. Suppl.* **26**, 126 (2007).
- [42] K. Karube, K. Shibata, J. S. White, T. Koretsune, X. Z. Yu, Y. Tokunaga, H. M. Rønnow, R. Arita, T. Arima, Y. Tokura *et al.*, Controlling the helicity of magnetic skyrmions in a β -Mn-type high-temperature chiral magnet, *Phys. Rev. B* **98**, 155120 (2018).
- [43] F. R. de Boer, C. J. Schinkel, J. Biesterbos, and S. Proost, Exchange-enhanced paramagnetism and weak ferromagnetism in the Ni_3Al and Ni_3Ga phases; giant moment inducement in Fe-doped Ni_3Ga , *J. Appl. Phys.* **40**, 1049 (1969).
- [44] M. K. Chattopadhyay and S. B. Roy, Metamagnetic transition and the anomalous virgin magnetization curve in $\text{Ce}(\text{Fe}_{0.96}\text{Ru}_{0.04})_2$, *J. Phys.: Condens. Matter* **20**, 025209 (2008).
- [45] M. A. Manekar, S. Chaudhary, M. K. Chattopadhyay, K. J. Singh, S. B. Roy, and P. Chaddah, First-order transition from antiferromagnetism to ferromagnetism in $\text{Ce}(\text{Fe}_{0.96}\text{Al}_{0.04})_2$, *Phys. Rev. B* **64**, 104416 (2001).
- [46] C. A. Cardoso, F. M. Araujo-Moreira, V. P. S. Awana, E. Takayama-Muromachi, O. F. de Lima, H. Yamauchi, and M. Karppinen, Spin glass behavior in $\text{RuSr}_2\text{Gd}_{1.5}\text{Ce}_{0.5}\text{Cu}_2\text{O}_{10-\delta}$, *Phys. Rev. B* **67**, 020407(R) (2003).
- [47] P. N. Lekshmi, G. R. Raji, M. Vasundhara, M. R. Varma, S. Savitha Pillai, and M. Valant, Re-entrant spin glass behaviour and magneto-dielectric effect in insulating $\text{Sm}_2\text{NiMnO}_6$ double perovskite, *J. Mater. Chem. C* **1**, 6565 (2013).
- [48] S. Giri, M. Patra, and S. Majumdar, Exchange bias effect in alloys and compounds, *J. Phys.: Condens. Matter* **23**, 073201 (2011).
- [49] J. Kroder, K. Manna, D. Kriegner, A. S. Sukhanov, E. Liu, H. Borrmann, A. Hoser, J. Gooth, W. Schnelle, D. S. Inosov *et al.*, Spin glass behavior in the disordered half-Heusler compound IrMnGa , *Phys. Rev. B* **99**, 174410 (2019).
- [50] R. Kumar, P. Yanda, and A. Sundaresan, Cluster-glass behavior in the two-dimensional triangular lattice Ising-spin compound $\text{Li}_2\text{Mn}_3\text{O}_7$, *Phys. Rev. B* **103**, 214427 (2021).
- [51] R. C. Sahoo, Y. Takeuchi, A. Ohtomo, and Z. Hossain, Exchange bias and spin glass states driven by antisite disorder in the double perovskite compound LaSrCoFeO_6 , *Phys. Rev. B* **100**, 214436 (2019).
- [52] R. L. Stamps, Mechanisms for exchange bias, *J. Phys. D* **33**, R247 (2000).
- [53] J. Sharma and K. G. Suresh, Observation of giant exchange bias in bulk $\text{Mn}_{50}\text{Ni}_{42}\text{Sn}_8$ Heusler alloy, *Appl. Phys. Lett.* **106**, 072405 (2015).
- [54] A. K. Nayak, M. Nicklas, S. Chadov, C. Shekhar, Y. Skourski, J. Winterlik, and C. Felser, Large zero-field cooled exchange-bias in bulk Mn_2PtGa , *Phys. Rev. Lett.* **110**, 127204 (2013).
- [55] S. N. Kaul, W. Kettler, and M. Rosenberg, Electrical resistivity of amorphous $\text{Fe}_{82}\text{B}_{18-x}\text{Ge}_x$ alloys: Coherent electron-magnon scattering contribution, *Phys. Rev. B* **35**, 7153 (1987).
- [56] P. D. Babu, S. N. Kaul, L. Fernández Barquín, J. C. Gomez Sal, W. H. Kettler, and M. Rosenberg, Electronelectron interaction, quantum interference and spin fluctuation effects in the resistivity of Fe-rich Fe-Zr metallic glasses, *Int. J. Mod. Phys. B* **13**, 141 (1999).
- [57] M. Vasundhara, V. Srinivas, and V. V. Rao, Electronic transport in Heusler-type $\text{Fe}_2\text{VAl}_{1-x}\text{Mn}_x$ alloys ($M = \text{B, In, Si}$), *Phys. Rev. B* **77**, 224415 (2008).
- [58] E. Rozenberg, M. Auslender, I. Felner, and G. Gorodetsky, Low-temperature resistivity minimum in ceramic manganites, *J. Appl. Phys.* **88**, 2578 (2000).
- [59] Y. Xu, J. Zhang, G. Cao, C. Jing, and S. Cao, Low-temperature resistivity minimum and weak spin disorder of polycrystalline $\text{La}_{2/3}\text{Ca}_{1/3}\text{MnO}_3$ in a magnetic field, *Phys. Rev. B* **73**, 224410 (2006).
- [60] B. L. Al'tshuler and A. G. Aronov, Contribution to the theory of disordered metals in strongly doped semiconductors, *Zh. Eksp. Teor. Fiz.* **77**, 2028 (1979) [*Sov. Phys. JEPT* **50**, 968 (1979)].
- [61] A. Aronov, Fourteen years of quantum interference in disordered metals, *Phys. Scr.* **1993**, 28 (1993).

- [62] W. Niu, M. Gao, X. Wang, F. Song, J. Du, X. Wang, Y. Xu, and R. Zhang, Evidence of weak localization in quantum interference effects observed in epitaxial $\text{La}_{0.7}\text{Sr}_{0.3}\text{MnO}_3$ ultrathin films, *Sci. Rep.* **6**, 26081 (2016).
- [63] M. Ziese, Searching for quantum interference effects in $\text{La}_{0.7}\text{Sr}_{0.3}\text{MnO}_3$ films on SrTiO_3 , *Phys. Rev. B* **68**, 132411 (2003).
- [64] D. Bombor, C. G. F. Blum, O. Volkonskiy, S. Rodan, S. Wurmehl, C. Hess, and B. Büchner, Half-metallic ferromagnetism with unexpectedly small spin splitting in the Heusler compound Co_2FeSi , *Phys. Rev. Lett.* **110**, 066601 (2013).
- [65] B. Raquet, M. Viret, E. Sondergard, O. Cespedes, and R. Mamy, Electron-magnon scattering and magnetic resistivity in $3d$ ferromagnets, *Phys. Rev. B* **66**, 024433 (2002).
- [66] H. Yamada and S. Takada, Magnetoresistance of Antiferromagnetic Metals Due to s-d Interaction, *J. Phys. Soc. Jpn.* **34**, 51 (1973).
- [67] S. N. Kaul, Low-temperature magnetization and spin-wave excitations in amorphous Ni-rich transition-metalmetaloid alloys, *Phys. Rev. B* **27**, 5761 (1983).
- [68] S. N. Kaul and P. D. Babu, Detailed magnetization study of quenched random ferromagnets, I. Low-lying magnetic excitations, *Phys. Rev. B* **50**, 9308 (1994).